Low Power Consumption Distributed-Feedback Quantum Cascade Lasers Operating in Continuous-Wave Mode above 90℃ at $\lambda \sim 7.2\,\mu$m *

Yue Zhao(赵越), Jin-Chuan Zhang(张锦川)**, Zhi-Wei Jia(贾志伟), Ying-Hui Liu(刘颖慧), Ning Zhuo(卓宁), Shen-Qiang Zhai(翟慎强), Feng-Qi Liu(刘峰奇)**, Zhan-Guo Wang(王占国)

Key Lab of Semiconductor Materials Science, Institute of Semiconductors, Chinese Academy of Sciences, Beijing 100083

Beijing Key Laboratory of Low Dimensional Semiconductor Materials and Devices, Beijing 100083

(Received 26 August 2016)

We report on the design and fabrication of $\lambda \sim 7.2\,\mu$m distributed feedback quantum cascade lasers for very high temperature cw operation and low electrical power consumption. The cw operation is reported above 90°C. For a 2-mm-long and 10-μm-wide laser coated with high-reflectivity on the rear facet, more than 170 mW of output power is obtained at 20°C with a threshold power consumption of 2.4 W, corresponding to 30 mW with a threshold power consumption of 3.9 W at 90°C. Robust single-mode emission with a side-mode suppression ratio above 25 dB is continuously tunable by the heat sink temperature or injection current.

PACS: 42.55.Px, 42.60.Pk, 42.72.Ai DOI: 10.1088/0256-307X/33/12/124201

Distributed feedback (DFB) quantum cascade lasers (QCLs) have shown great potential in many areas such as high resolution spectroscopy, gas sensing and free space optical communication due to its narrow linewidth and tunable wavelength.[1–3] For compact and portable systems in particular, laser power consumption is always the limiting factor. Most of the spectroscopic techniques need mW level cw optical output power, and then it is possible to decrease the device dimensions significantly to reduce the electrical dissipation at the same time. Rapid progress in reducing the electrical power consumption of DFB QCLs has been made in recent years. In Ref. [4] they reported a cw threshold power consumption of 0.7 W, as carried out to be 0.76 W in Ref. [5] and 0.44 W in Ref. [6]. However, the threshold current densities of these devices all are higher than 1.5 kA/cm^2 due to the increased mirror loss induced by the short cavities. Thus the maximum operating temperature is usually below 50℃, which makes it difficult to apply in the humid environment. In fact, it is easy to make the temperature control for quantum cascade lasers (QCL) when the electrical power consumption is less than 5 W,[7–9] and the high optical power is always important for improving test sensitivity and distance.

In this Letter, we design and fabricate a strong coupled buried grating and use the regrowth technique to reduce DFB cavity loss to achieve a low power consumption and high operating temperature. The threshold current density of DFB QCL is 0.95 kA/cm^2, the threshold power consumption is 2.5 W and the output power is up to 170 mW at 20℃, for a 2-mm-long and 10-μm-wide laser coated with high-reflectivity (HR) on the rear facet. More than 30 mW of output power is obtained at a high operating temperature of 90℃, corresponding to the threshold power consumption of 3.9 W. Stable single-mode emission with a side-mode suppression ratio (SMSR) above 25 dB is continuously tunable by the heat sink temperature and the injection current.

The QCL structure designed according to the bound-to-continuum theory was grown on an n-doped (Si, 2×10^{17} cm^{-3}) InP substrate wafer by the solid-source molecular beam epitaxy (MBE). The active core presented in this study is resemblant of Ref. [10] containing 50 periods of strain-compensated $In_{0.6}Ga_{0.4}As/In_{0.44}Al_{0.56}As$ quantum wells and barriers. The specific layer sequence in one period is (layer thickness in nanometers): **4.0**/1.8/**0.8**/5.3/**1.0**/4.8/**1.1**/4.3/**1.4**/3.6/**1.7**/3.3/**2.4**/3.1/**3.4**/2.9, the bold represents barrier $In_{0.44}Al_{0.56}As$ layers. The complete structure of the QCL wafer layer sequence is: 4 μm lower InP cladding (Si, 8×10^{16} cm^{-3}), 0.3-μm-thick n-$In_{0.53}Ga_{0.47}As$ layer (Si, 4×10^{16} cm^{-3}), 50 active/injector stages, 0.3-μm-thick n-$In_{0.53}Ga_{0.47}As$ layer (Si, 4×10^{16} cm^{-3}), 2.6 μm upper cladding (Si, 3×10^{16} cm^{-3}), 0.15 μm gradually doped (changing from 1×10^{17} to 3×10^{17}cm^{-3}) and 0.8 highly doped cladding (Si, 5×10^{18} cm^{-3}).

To achieve a low threshold current density and narrow linewidth device, the buried grating needs to obtain low mode loss and high coupling coefficient κ. We have simulated the coupling coefficient changing

*Supported by the National Basic Research Program of China under Grant No 2013CB632801, the National Key Research and Development Program under Grant No 2016YFB0402303, the National Natural Science Foundation of China under Grant Nos 61435014, 61627822, 61574136 and 61306058, the Key Projects of Chinese Academy of Sciences under Grant No ZDRW-XH-2016-4, and the Beijing Natural Science Foundation under Grant No 4162060.

**Corresponding author. Email: zhangjinchuan@semi.ac.cn; fqliu@semi.ac.cn

© 2016 Chinese Physical Society and IOP Publishing Ltd

with the increase of the grating depth at a fixed duty cycle of $\sigma = 0.4$ and a grating period of $\Lambda = 1.134\,\mu\text{m}$ based on the finite element method under periodical boundary conditions. The coupling coefficient of two modes (denoted as modes 1 and 2) that changed with the depth of grating is shown in Fig. 1, which increases with the depth of grating approaching linearly. A grating depth of 120 nm will generate a coupling coefficient of $\kappa = 17.6\,\text{cm}^{-1}$, considering a high-reflectivity coated 2-mm-long cavity, the coupling strength $\kappa L = 7.04$ proves that there is enough outcoupling efficiency.

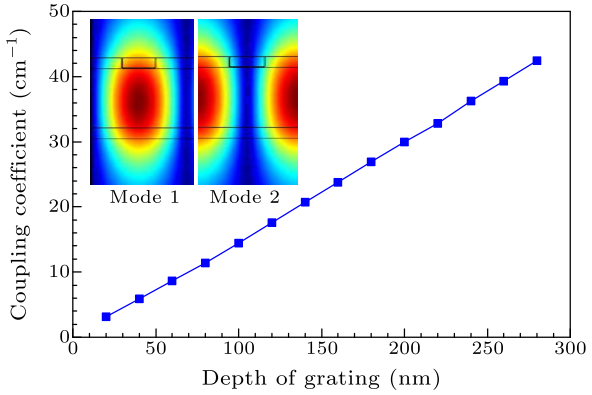

Fig. 1. Coupling coefficient of two modes (modes 1 and 2) as a function of the depth of grating. A duty cycle of $\sigma = 0.4$ is used in the simulation. The inset shows the modal profile of modes 1 and 2 at a grating depth of 120 nm.

A period of $\Lambda = 1.134\,\mu\text{m}$ (duty cycle $\sigma = 0.4$) first-order grating was defined on the InGaAs layer by a holographic lithography technique and transferred by wet chemical etching to 120 nm deep. The QCL wafer was then processed into the double-channel ridge waveguide laser with an average active core width of 10 μm by conventional photolithography and a nonselective wet chemical etching using $HBr/HCl/H_2O_2/H_2O$ solution. After etching the grating and double-channel, InP cladding was epitaxied by a metal organic chemical vapor deposition as the upper waveguide. A layer of 450-nm-thick SiO_2 served as an electrical insulation around the laser ridges and was deposited by plasma enhanced chemical vapor deposition (PECVD). Then the Ti/Au layer was deposited by e-beam evaporation as top contacts, followed by a 5-μm-thick Au layer electroplated to better conduct the current and heat on the laser surface. After the wafer was thinned down to 80 μm, the Ge/Au/Ni/Au metal contacts were formed as the substrate layer. Lastly, the wafer was cleaved to 2-mm-long laser bars and HR coating consisting of $Al_2O_3/Ti/Au/Ti/Al_2O_3$ (200 nm/10 nm/100 nm/10 nm/120 nm) was deposited on the rear facet.

The lasers were mounted on the epilayer side down onto copper heat sinks with indium solder. Then the devices were wire bonded and a thermistor was mounted on the heat sinks very close to the laser to monitor the temperature of heat sinks. The heat sink was then fixed on a metal sheet, of which the temperature was monitored and adjusted with a thermistor and a thermoelectric cooler (TEC). The temperature of heat sink is controlled very close to the metal sheet under cw operation at 20–90℃. Due to the limitation of the measurement setup, devices were not tested at the maximum operating temperature. The optical power from the uncoated facet of the laser was measured with a calibrated thermopile detector placed directly in front of the laser facet. The laser spectra were measured with a Fourier transform infrared (FTIR) spectrometer in rapid scan mode with a resolution of 0.25 cm^{-1}.

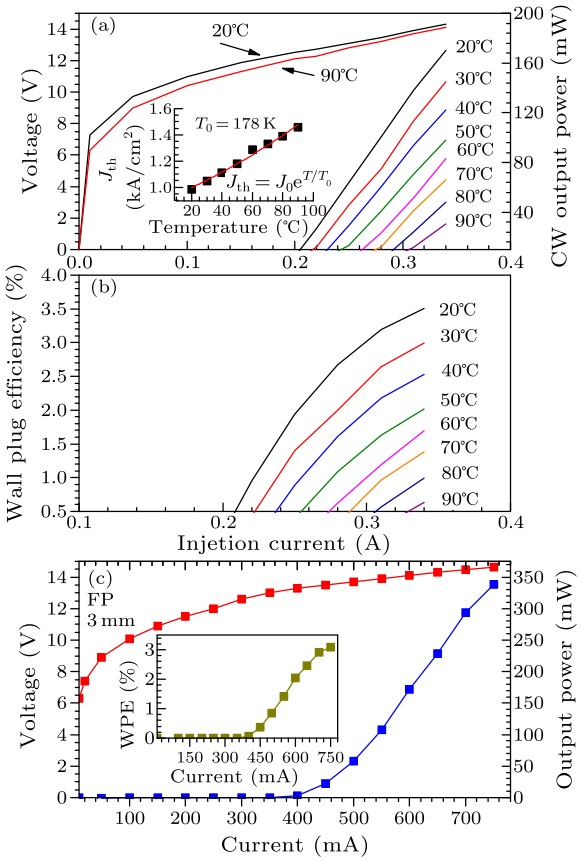

Fig. 2. (a) Output light power versus the injection current of a 2-mm-long and 10-μm-wide DFB QCL in the cw operation mode at different heat sink temperatures between 20℃ and 90℃ along with V–I curves at 20℃ and 90℃. The inset shows the threshold characteristic change as a function of the temperature, which can be fitted to $J_{th} = J_0 \exp(T/T_0)$, with $T_0 = 178$ K. (b) Wall plug efficiency versus the injection current of the same devices between 20℃ and 90℃. (c) Output light power versus the injection current of a 3-mm-long and 10-μm-wide FP QCL in cw operation mode with a V–I curve at 20℃, the inset shows the wall plug efficiency versus the injection current of the devices at 20℃.

Figure 2(a) shows the optical power-current-voltage (PIV) curve of a 10-μm-wide and 2-mm-long

coated HR on the rear facet DFB QCL, operating at different heat sink temperatures from 20 to 90℃. A low threshold current density ($J_{\rm th}$) of 0.95 kA/cm^2 is obtained with a high optical output power of 170 mW at 20℃. Compared with other DFB QCLs at 7.x μm in Refs. [8,11,12], these are better output power and operating temperature that have been reported. With the temperature up to 90℃, the threshold current density increases to only 1.46 kA/cm^2 with the cw output power decreasing to 30 mW still. The threshold electrical power consumption is 2.5 W at 20℃ and increases to only 3.9 W at 90℃. The inset shows the temperature dependence of the threshold characteristic, which can be fitted by the expression $J_{\rm th} = J_0 \exp(T/T_0)$. The dotted line is the fitting result. Between 293 and 363 K, the characteristic temperature T_0 is 178 K with $J_0 = 0.89$ kA/cm^2. Figure 2(b) shows the wall plug efficiency (WPE) changing with the current between 20℃ and 90℃, the high efficiency of 3.5% is obtained at 20℃ and still 2% at 50℃. The maximum WPE is higher than those in Ref. [4–6], which are all less than 1%. Figure 2(c) shows the PIV curve of a 3-mm-long and 10-μm-wide FP device, the high output power of 328 mW is obtained at 750 mA with the WPE of 3.1%. The threshold of FP QCL is 400 mA and the threshold current density is 1.33 kA/cm^2.

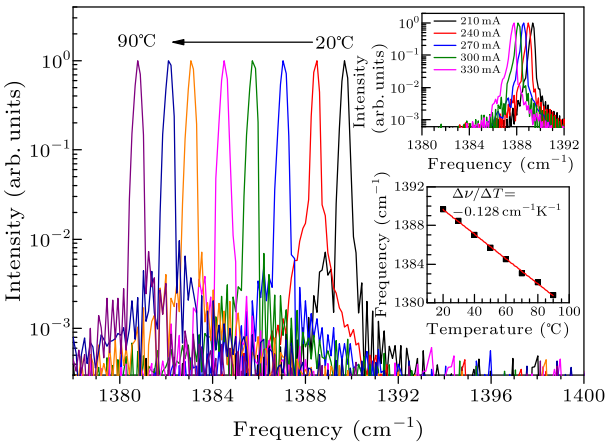

Fig. 3. The cw emitting spectra of DFB QCL at different heat sink temperatures between 20℃ and 90℃. The lower inset shows the linear-fit tuning characteristics of the lasing frequency with temperature for the same device. The upper inset shows the cw lasing spectra at different injection currents from 0.21 A to 0.33 A with steps of 0.03 A.

Figure 3 shows the normalized cw lasing spectra at current of 1.02$I_{\rm th}$ in the temperature range from 20℃ to 90℃ with steps of 10℃ of the DFB QCL. Single-mode emission with SMSR about 25 dB is obtained in the whole temperature range. The single lasing mode wavelength changes from 1389.7 cm^{-1} at 20℃ to 1380.6 cm^{-1} at 90℃ with the temperature tuning coefficient $\Delta\nu/\Delta T$ of -0.128 cm^{-1}K^{-1}, as shown in the lower inset. The upper inset demonstrates the cw lasing spectra of the same device at different injection currents, from 0.21 to 0.33 A, with steps of 0.03 A at 20℃. Due to the high coupling coefficient, the stable single-mode emission was achieved even at the full power current.

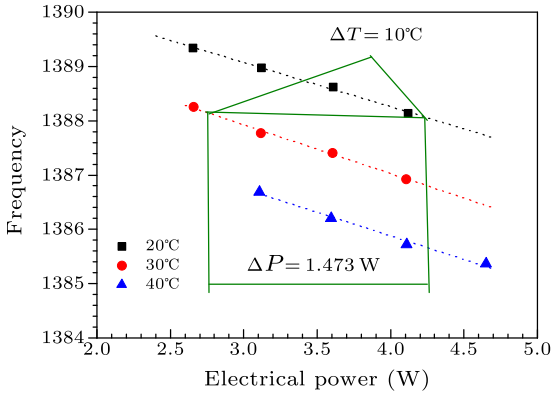

Fig. 4. Lasing frequency changes as a function of the input electrical power at different temperatures between 20℃ and 40℃. The dotted lines are fitted with the function $\nu = \nu_0 + \beta\nu T_{\rm heatsink} + \beta\nu R_{\rm th} P_{\rm elec}$.

DFB QCL lasing frequency changes as a function of the input electrical power in a particular temperature, corresponding to the correlation between the lasing frequency and the input electrical power can be expressed by $\nu = \nu_0 + \beta\nu T_{\rm heatsink} + \beta\nu R_{\rm th} P_{\rm elec}$, where $\beta = (1/\nu)(\Delta\nu/\Delta T)$ is the thermal tuning coefficient, ν is the wavenumber, $P_{\rm elec}$ is the electrical power, $T_{\rm heatsink}$ is the heat sink temperature, and $R_{\rm th}$ is the heat resistance. Lasing frequency varying with the electrical power was measured and fitted in Fig. 4. For a given frequency, the electrical power changes 1.472 W when the temperature changes 10℃. Considering the equation between frequency and electrical power, it gives $\nu(T_2, P_2) - \nu(T_1, P_1) = \beta\nu\Delta T_{\rm heatsink} + \beta\nu R_{\rm th}\Delta P_{\rm elec} = 0$, resulting in $R_{\rm th} = \Delta T_{\rm heatsink}/\Delta P_{\rm elec} = 6.79$ K/W (the thermal conductance $G_{\rm th} = 1/R_{\rm th}A = 736.4$ W/Kcm^2). The value of $\beta = -9.11 \times 10^{-5}$ K^{-1} is estimated from fitting the experimental results by using the above function. The small thermal resistance value is mainly caused by the epi-down bonding and low electrical power consumption.

Figure 5 shows the uncooled cw output power versus the injection current of the same device at an environment temperature of 298 K. For uncooled operation of DFB QCLs, the chip was also mounted on a metallic copper heat sink, while without a TEC. The maximum cw output power is 112 mW with a low threshold current density of 1.1 kA/cm^2. The threshold electrical power consumption is only 2.8 W and increases to only 4.9 W at the maximum optical power under the uncooled condition. The inset shows that the heat sink temperature increases with the electrical power. It can be seen that the heat sink temperature has a nearly linear correlation with the increase of the

injection electrical power after the devices lasing. The temperature changes from 305 K to 312 K, only increased by ∼7 K. For the device reported here, the additional thermal resistance $R_{\rm th} = 2.97\,{\rm K/W}$ is deduced from the inset of Fig. 5.

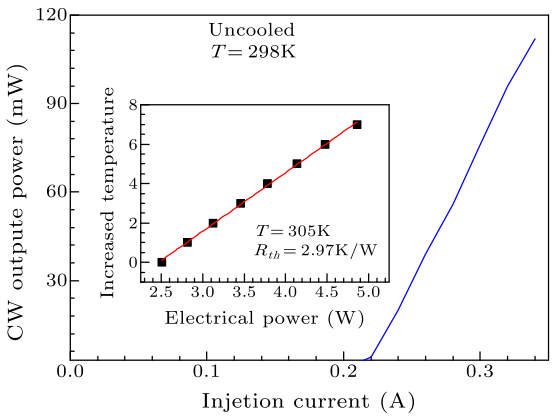

Fig. 5. The output power versus the injection current of an uncooled cw QCL. The inset shows that the heat sink temperature increases with the injection electrical power.

In conclusion, we have designed and fabricated a low power consumption and high operating temperature DFB QCL at $\lambda \sim 7.2\,\mu{\rm m}$, aiming at special environment operating portable gas sensing applications. A single-mode cw output power of greater than 30 mW at 90℃ is obtained with the current density of $1.46\,{\rm kA/cm^2}$, better than previously published results for mid-IR DFB QCLs.

References

[1] Namjou K, Cai S, Whittaker E A et al 1998 *Opt. Lett.* **23** 219
[2] Kosterev A and Tittel F 2002 *Quantum Electron.* **38** 582
[3] Liu C W, Zhai S Q, Zhang J C et al 2015 *J. Semicond.* **36** 85
[4] Hinkov B, Bismuto A, Bonetti Y, Beck M, Blaser S and Faist J 2012 *Electron. Lett.* **48** 646
[5] Briggs R M, Frez C, Borgentun C E and Forouhar S 2014 *Appl. Phys. Lett.* **105** 14117
[6] Razeghi M, Tournié E, Brown G J et al 2015 *Proc. SPIE* **9370** 93700F
[7] Xie F, Caneau C G, Leblanc H P et al 2009 *Appl. Phys. Lett.* **95** 091110
[8] Zhang J C, Liu F Q, Tan S et al 2012 *Appl. Phys. Lett.* **100** 112105
[9] Yan F L, Zhang J C, Yao D Y et al 2015 *Chin. Phys.* B **24** 024212
[10] Bismuto A, Terazzi R, Beck M and Faist J 2010 *Appl. Phys. Lett.* **96** 141105
[11] Darvish S, Zhang W, Evans A et al 2006 *Appl. Phys. Lett.* **89** 251119
[12] Briggs R M, Frez C, Fradet M et al 2016 *Opt. Express* **24** 14589